Cytidine Derivatives as SARS-CoV-2 Mpro Inhibitors: Antiviral Prediction, Molecular Docking and Pharmacokinetic Score Investigations

Sarkar Mohammad Abe Kawsar (akawsar@cu.ac.bd)
University of Chittagong
Mohammed Anowar Hosen
University of Chittagong
Yuki Fujii
Nagasaki International University: Nagasaki Kokusai Daigaku
Yasuhiro Ozeki
Yokohama City University: Yokohama Shiritsu Daigaku

Research Article

Keywords: Cytidine, Antiviral, SARS-COV-2 Mpro, Molecular Docking, Pharmacokinetic

Posted Date: July 30th, 2021

DOI: https://doi.org/10.21203/rs.3.rs-741343/v1

Abstract

Severe acute respiratory syndrome coronavirus 2 (SARS-CoV-2) is a beta coronavirus that was first found during the Wuhan COVID-19 epidemic in 2019 and is listed as a potential global health threat by World Health Organization due to its high mortality. The main protease of SARS-CoV-2 is one of the optimum targets for antiviral drug design and development. Nucleoside derivatives have been investigated since many years, and some of the most clinically effective antiviral agents used currently include purine or pyrimidine nucleoside derivatives. In this study, the hydroxyl (–OH) groups of cytidine structures were modified with different aliphatic and aromatic groups to obtain 5´-*O*-acyl and 2´,3´-di-*O*-acyl derivatives, and then, these derivatives were employed for molecular modeling, molecular docking, antiviral prediction, and pharmacological studies. Density functional theory at the B3LYP/3-21G level was employed to analyze the thermochemical stability and molecular electrostatic potential of the modified derivatives to evaluate the effect of the aliphatic and aromatic groups on the drug properties. All the derivatives were more stable than their parent molecule, cytidine. The experimental and computed IR analyses showed the characteristic peaks for various aliphatic and aromatic groups. The antiviral parameters of the modified derivatives revealed promising drug properties compared with those of standard antiviral drugs. Molecular docking was performed using AutoDock Vina to determine binding affinities and interactions between the cytidine derivatives and SARS-CoV-2 main protease. The modified derivatives strongly interacted with prime Cys145 and His41 residues. Finally, the pharmacokinetic characterization of the optimized inhibitors showed the derivatives to be safe due to their improved kinetic properties. Our comprehensive computational and statistical analyses showed that the selected cytidine derivatives can be used as potential inhibitors against SARS-CoV-2.

1 Introduction

Nucleoside agents (NAs) are the subunits of DNA and RNA and comprise a sugar moiety connected to a nitrogen base through an *N*-β-glycosidic bond [1]. NAs have considerable clinical importance as medicinal agents due to their antiviral and anticancer activities [2] and are the drugs of choice for treating various viral diseases, such as herpes simplex (HSV-1), human cytomegalovirus, varicella-zoster, human immunodeficiency virus (HIV) type-1, human hepatitis B (HBV) and C (HCV) [3], ebola [4], dengue [5], and Zika [6]. Additionally, 2′-deoxynucleosides such as doxuridne, trifluridine, doxudine, vidarabine, and brivudine are used to treat herpes virus infections [7,8]. Certain 2′,3′-dideoxynucleosides such as zidovudine, didanosine, zalcitabine, stavudine, and abacavir are the most effective therapeutic agents against HIV [9]. Modifications in sugar moieties, such as ribofuranose or deoxyribofuranose of nucleosides, include changes in sugar substituents, the replacement of oxygen with another atom, the addition of a heteroatom in the sugar ring, ring size variations, and replacement with an acyclic moiety [10–15]. These alterations may lead to excellent variations in the biological activity and degree of selective toxicity according to the respective chemical and physical properties of the moieties [16–22]. The modified compounds exhibit a broad-spectrum biological activity. For example, zidovudine with an azido group at 3′-position is used to treat HIV. Thymidine (**1**) derivatives such as telbivudine are antiviral drugs are used in HBV treatment [23]. Azidothymidine (3′-azido-2′,3′-dideoxythymidine) is another thymidine analog used in HIV treatment. The supplementation of dietary cytidine (5´)-diphosphocholine protects against the development of memory deficits [24]. Cytidine is present in organ meats and pyrimidine-rich foods such as beer, tomatoes, broccoli, and oats. Cytidine is an RNA component that transfers instructions from DNA to proteins [25]. When RNA levels decrease, cytidine is supplemented to maintain high RNA levels for a high memory function. Another important function of cytidine is to increase dopamine production and release it in the brain. Cytidine is a powerful neurotransmitter responsible for regulating functions, such as mood and movement control.

Nucleoside analogs and nucleobases constitute a pharmacologically diverse family, which includes cytotoxic compounds, antiviral agents, and immune suppressive molecules [26–29]. Cytidine analog 5-AZA-2´-deoxycytidine is utilized to control the growth of neuroblastoma malignant tumors [30]. Cytidine analog KP-1461 is an anti-HIV agent that acts as a viral mutagen [31]. Various cytidine derivatives modified at the base or ribose exhibit antiviral or antitumor activities.

The recent outbreak of the novel coronavirus disease (COVID-19), caused by a severe acute respiratory syndrome (SARS)-like coronavirus, that started in Wuhan, China, is spreading rapidly in humans; this outbreak is now considered a global pandemic [32]. Modifications of the hydroxyl (–OH) group of the nucleoside structure showed some potent SARS-CoV-2 candidates [33–

34] and antimicrobial agents. The COVID-19 outbreak caused by the new coronavirus, which appeared in China, remains a serious problem worldwide. Although SARS-CoV and SARS-CoV-2 agents belong to beta-coronaviruses category, they slightly differ from each other. Studies have shown that SARS-CoV-2 shares 80% nucleotide identity and 89.10% nucleotide similarity with SARS-CoV. Thus, the main protease of SARS-CoV, $3CL^{pro}$, is the target of several *in silico* investigations for developing potential inhibitor candidates. Between nCoV and nCoV2, $3CL^{pro}$ provides a high sequence identity rate; hence, their $3CL^{pro}$ is likely homologous and has similar structure and functions. Furthermore, SARS-CoV and SARS-CoV-2 affect cells in the same manner and employ the same protein machinery to enhance inside the host cell. Due to their features, we explored the molecular electrostatic potential (MEP) and biochemical behavior of several previously synthesized cytidine derivatives by conducting the quantum mechanical study. The infrared (IR) spectrum was measured through optimization and frequency calculation to compare it with experimental IR spectra, which confirmed the insertion of various functional groups. Furthermore, all the derivatives were employed for molecular docking against SARS-CoV-2 main protease protein (PDB: 6LU7) to understand their nonbonding interactions, binding mode, and binding affinity and to predict their antiviral properties. Pharmacokinetic properties were investigated to compare their absorption, lipophilicity, and solubility, and a radar map was utilized to understand their biological acceptance.

2 Experimental

2.1 Materials and Methods

To identify drug interactions with receptor proteins, molecular docking is the optimum tool. In the blind docking method, the overall surface of the protein molecule was thoroughly analyzed for binding sites. The following software tools were used in this study to predict antiviral properties: i) Gaussian 09, ii) AutoDock 4.2.6, iii) Swiss-Pdb 4.1.0, iv) Python 3.8.2, v) Discovery Studio 4.1, vi) PyMOL 2.3, vii) http://crdd.osdd.net/servers/avcpred. Moreover, admetSAR server (http://lmmd.ecust.edu.cn/admetsar2/about), and SwissADME free web tools (http://www.swissadme.ch) were employed to calculate the pharmacokinetic properties.

2.2 Antiviral Activity Determination

Antiviral molecules (AVMs) present a category of antimicrobial drugs used to treat viral infections by inhibiting the growth of viral pathogens inside the host cells. For antiviral activity calculation, we used online software (http://crdd.osdd.net/servers/avcpred), which showed the inhibitory percentage. The SD (sampled data) file format of the cytidine derivatives was entered as input for predications. The derivatives were assessed for the development of antiviral therapeutics and suggesting the optimal inhibitory cytidine derivatives for further studies.

2.3 Chemical Reactivity and IR Optimization

In a computer-based drug design, thermal, molecular orbital, and molecular electrostatic features are widely calculated using the quantum mechanical method [35]. The geometrical calculation and subsequent alteration of all the cytidine derivatives were conducted using Gaussian 09 program [36]. The IR frequency and spectral properties of the cytidine derivatives were optimized and calculated employing density functional theory (DFT)-based force field with Beck's (B) three-feature hybrid model and Lee, Yang, and Parr's correlation functional by using basis set 3-21G [37, 38].

2.4 Pharmacokinetic Prediction

In drug development, ADMET (absorption, distribution, metabolism, excretion, and toxicity) property prediction is crucial to prevent drug failure in clinical stages. Thus, the designed derivatives were evaluated for their *in silico* pharmacokinetics parameters to prevent their failure during clinical trials and improve their candidacy as potential candidate drugs. Online server admetSAR was employed to calculate the pharmacokinetic properties of the designed cytidine derivatives and parent compounds. We used the online database, admetSAR, to evaluate the pharmacokinetics profile involved in the drug lipophilicity, toxicity, and absorption of cytidine and its selected analogs [39]. By using the structural resemblance exploration methodology, admetSAR predicted the latest and most widespread, manually curated results for several chemicals related to the studied

ADMET profiles. For ADMET calculation, admetSAR was employed, in which 96,000 sole compounds (including 45 types of ADMET-related parameters), proteins, species, and organisms are diligently curated from various studies.

2.5 Protein Selection and Molecular Docking

The 3D crystal format of SARS-CoV-2 main protease protein (pdb: 6LU7) was recuperated in pdb from the protein data bank [40]. PyMol (version 1.3) software packages were used to eliminate all the heteroatoms and water molecules [41]. Protein energy was minimized using Swiss-PdbViewer (version 4.1.0) [42]. Furthermore, a molecular docking study was conducted against the SARS-CoV-2 main protease protein 6LU7 (Fig. 1) for the optimized drugs. Finally, PyRx application (version 0.8) was used for molecular docking simulations [43], which envisaged the target protein and cytidine derivatives as a macromolecule and ligand, respectively. The protein and ligands were entered as input by converting the pdb format to pdbqt format by using AutoDock tools of the MGL software package. In AutoDockVina, the grid box size was maintained at 51.3565, 66.9335, and 59.6050 Å along the X-, Y-, and Z-axis. After docking, both the macromolecule and ligand structures were saved in the pdbqt format. and Accelrys Discovery Studio (version 4.1) was employed to analyze the docking results and predict the nonbonding interactions among the cytidine derivatives and amino acid chains of receptor proteins [44]. PROCHECK online server was used for validation 92.06 overall quality factor was obtained in ERRAT (http://www.ncbi.nlm.nih.gov/entrez/query.fcgi?cmd=Retrieve&db=PubMed&list_uids=8401235&dopt=Abstract), and 93.10% score was acquired in VERIFY 3D (https://www.ncbi.nlm.nih.gov/pubmed/1853201?dopt=Abstract). PDBsum online server was used to validate the main protease receptor with the Ramachandran plot and ligplot (Fig. 2), which indicated 90.6% residue in the allowed region, and no residues were missed.

3 Results And Discussion

In this study, 14 cytidine esters were modified with different aliphatic and aromatic chains (**2**–**15**) (Table 1) and were geometrically optimized to realize the modes of their antimicrobial behavior. Initially, partial acylated derivatives were selected for antiviral activities using the online web tool. Subsequently, the observed activities were rationalized by measuring the IR frequency, physicochemical properties, molecular docking, *in silico* pharmacokinetics, and drug-likeness properties. In nucleoside chemistry, the selective alteration of certain hydroxyl groups is important because the resulting acylation products might be useful precursors for the synthesis of new, bioactive products. Moreover, the designed acyl derivatives might exhibit a high antiviral efficacy as versatile intermediates for synthesizing various other antiviral drugs of fundamental importance.

3.1 Structural Identification of the Designed Cytidine Derivatives

Table 1 and Fig. 3 present the atomic identification and structural variations of the substituted cytidine derivatives. Different aliphatic (pivaloyl, hexanoyl, octanoyl, decanoyl, laouroyl palmitoyl, myristoyl, and steroyl) and aromatic (4-chlorobenzoyl, cinnamoyl, 4-tert-butylbenzoyl, and trityl) groups were subjected to the hydroxyl (–OH) group modification of cytidine for investigating the variations in biological activities.

Table 1
Structural views of the cytidine derivatives with SMILES

Compounds	Molecular formula	Molecular weight	Compounds name	SMILES
1	$C_9H_{13}N_3O_5$	242.22	Cytidine	NC1 = NC(= O)N(C = C1)C1OC(CO)C(O)C1O
2	$C_{19}H_{31}N_3O_6$	397.47	5′-*O*-Decanoylcytidine	CCCCCCCCCC(= O)OCC1OC(C(O)C1O)N1C = CC(N) = NC1 = O
3	$C_{35}H_{59}N_3O_8$	649.87	5′-*O*-Decanoyl-2′,3′-di-*O*-octanoylcytidine	CCCCCCCCCC(= O)OCC1OC(C(OC(= O)CCCCCCC)C1OC(= O)CCCCCCC)N1C = CC(N) = NC1 = O
4	$C_{51}H_{91}N_3O_8$	874.30	5′-*O*-Decanoyl-2′,3′-di-*O*-palmitoylcytidine	CCCCCCCCCCCCCCCC(= O)OC1C(COC(= O)CCCCCCCCC)OC(C1OC(= O)CCCCCCCCCCCCCCC)N1C = CC(N) = NC1 = O
5	$C_{55}H_{99}N_3O_8$	929.86	5′-*O*-Decanoyl-2′,3′-di-*O*-stearoylcytidine	CCCCCCCCCCCCCCCCCC(= O)OC1C(COC(= O)CCCCCCCCC)OC(C1OC(= O)CCCCCCCCCCCCCCCCC)N1C = CC(N) = NC1 = O
6	$C_{57}H_{59}N_3O_6$	882.11	5′-*O*-Decanoyl-2′,3′-di-*O*-(triphenylmethyl)cytidine	CCCCCCCCCC(= O)OCC1OC(C(OC(C2 = CC = CC = C2)(C2 = CC = CC = C2)C2 = CC = CC = C2)C1OC(C1 = CC = CC = C1)(C1 = CC = CC = C1)C1 = CC = CC = C1)N1C = CC(N) = NC1 = O
7	$C_{41}H_{55}N_3O_8$	717.90	5′-*O*-Decanoyl-2′,3′-(4-*tert*-butylbenzoyl)cytidine	CCCCCCCCCC(= O)OCC1OC(C(OC(= O)C2 = CC = C(C = C2)C(C)(C)C)C1OC(= O)C1 = CC = C(C = C1)C(C)(C)C)N1C = CC(N) = NC1 = O
8	$C_{28}H_{27}N_3O_5$	485.54	5′-*O*-(Triphenylmethyl)cytidine	NC1 = NC(= O)N(C = C1)C1OC(COC(C2 = CC = CC = C2)(C2 = CC = CC = C2)C2 = CC = CC = C2)C(O)C1O
9	$C_{40}H_{47}N_3O_7$	681.83	2′,3′-Di-*O*-hexanoyl-5′-*O*-(triphenylmethyl)cytidine	CCCCCC(= O)OC1C(COC(C2 = CC = CC = C2)(C2 = CC = CC = C2)C2 = CC = CC = C2)OC(C1OC(= O)CCCCC)N1C = CC(N) = NC1 = O
10	$C_{42}H_{53}N_3O_7$	709.87	2′, 3′-Di-*O*-heptanoyl-5′-*O*-(triphenylmethyl)cytidine	CCCCCCC(= O)OC1C(COC(C2 = CC = CC = C2)(C2 = CC = CC = C2)C2 = CC = CC = C2)OC(C1OC(= O)CCCCCC)N1C = CC(N) = NC1 = O
11	$C_{52}H_{71}N_3O_7$	850.15	2′,3′-Di-*O*-lauroyl-5′-*O*-(triphenylmethyl)cytidine	CCCCCCCCCCCC(= O)OC1C(COC(C2 = CC = CC = C2)(C2 = CC = CC = C2)C2 = CC = CC = C2)OC(C1OC(= O)CCCCCCCCCCC)N1C = CC(N) = NC1 = O
12	$C_{56}H_{79}N_3O_7$	906.26	2′,3′-Di-*O*-myristoyl-5′-*O*-(triphenylmethyl)cytidine	CCCCCCCCCCCCCC(= O)OC1C(COC(C2 = CC = CC = C2)(C2 = CC = CC = C2)C2 = CC = CC = C2)OC(C1OC(= O)CCCCCCCCCCCC)N1C = CC(N) = NC1 = O
13	$C_{38}H_{43}N_3O_7$	653.77	2′,3′-Di-*O*-pivaloyl-5′-*O*-(triphenylmethyl)cytidine	CC(C)(C)C(= O)OC1C(COC(C2 = CC = CC = C2)(C2 = CC = CC = C2)C2 = CC = CC = C2)OC(C1OC(= O)C(C)(C)C)N1C = CC(N) = NC1 = O
14	$C_{42}H_{33}N_3O_7Cl_2$	762.64	2′,3′-Di-*O*-(4-chlorobenzoyl)-5′-*O*-(triphenylmethyl) cytidine	NC1 = NC(= O)N(C = C1)C1OC(COC(C2 = CC = CC = C2)(C2 = CC = CC = C2)C2 = CC = CC = C2)C(OC(= O)C2 = CC = C(Cl)C = C2)C1OC(= O)C1 = CC = C(Cl)C = C1
15	$C_{46}H_{36}N_3O_7$	742.80	2′,3′-Di-*O*-cinnamoyl-5′-*O*-(triphenylmethyl)cytidine	NC1 = NC(= O)N(C = C1)C1OC(COC(C2 = CC = CC = C2)(C2 = CC = CC = C2)C2 = CC = CC = C2)C(OC(= O)\C = C/C2 = CC = CC = C2)C1OC(= O)\C = C/C1 = CC = CC = C1

Antiviral Activity Prediction

When considerable antimicrobial and anti-carcinogenic activities were acquired, we predicted the antiviral activities of cytidine derivatives (**2–15**) and compared them with those of azidothymidine (AZT, antiviral drug) and remdesivir (COVID-19 drug) by using an antiviral application (Table 2) [45].

Table 2
Predicted antiviral activities (% inhibition) of cytidine derivatives **2–15**, remdesivir, and AZT

Compounds	General	HBV	HCV	HHV	HIV
1	-	-	-	-	-
2	56.694	24.616	52.294	39.139	60.776
3	50.334	25.168	44.745	68.231	69.760
4	51.770	25.164	44.746	65.844	70.174
5	7.689	20.217	18.367	48.010	71.148
6	5.209	22.034	17.707	32.962	62.485
7	8.964	19.478	38.064	46.137	65.673
8	54.817	25.306	58.732	51.525	55.146
9	2.101	19.505	44.539	44.016	68.671
10	2.327	19.694	37.089	45.767	68.719
11	50.134	24.790	47.106	60.254	62.961
12	4.310	20.681	37.091	43.999	69.047
13	3.345	19.376	56.274	81.466	65.758
14	47.021	26.981	46.291	75.321	63.214
15	61.039	18.367	53.816	61.409	63.427
Remdesivir	48.642	22.443	66.968	36.291	69.503
AZT	87.038	19.619	24.962	28.728	92.855

HBV = Hepatitis B virus; HCV = Hepatitis C virus; HHV = Human herpesvirus; HIV = Human immunodeficiency virus.

The predicted antiviral activities revealed that the modified cytidine derivatives (**2–15**) exhibit potential antiviral efficacy compared with their parent molecules. The aliphatic derivatives (**2–4**) and aromatic derivatives (**8**, **11, 14**, and **15**) exhibited more promising scores than aliphatic derivatives (**3–5**) along with standard drugs remdesivir and azidothymidine (AZT).

Computed and Experimental IR Spectrum for Characterization

The IR spectrum, which indicated the characteristic peaks for various functional groups, was calculated through optimization and frequency calculation by using Gaussian software 09 packet. In the modified cytidine derivatives, various aliphatic chains (pivaloyl, hexanoyl, octanoyl, decanoyl, laouroyl palmitoyl, myristoyl, and steroyl) and aromatic (4-chlorobenzoyl, cinnamoyl, 4-tert-butylbenzoyl, and trityl) groups were introduced. In some functional groups, such as CH_3, CO and NH_3, where the C–C, C–H, C–N, C = O, and N–H stretching vibrations were observed (Fig. 4).

For derivatives (**2**) and (**8**), where primary hydroxyl (–OH) was modified with decanoyl and trityl groups, peaks appeared at approximately 1730 and 1720 cm^{-1} for –CO stretching, 3420–3500 cm^{-1} for –OH stretching, and 3545 cm^{-1} due to –NH stretching. For derivatives (**3–5**) and (**9–13**), where the secondary hydroxyl (–OH) groups were substituted with different

aliphatic chains (C5–C18), the IR spectra displayed absorption bands at 1715–1730 and 3450–3480 cm^{-1} for C = O and –NH stretching, respectively. Finally, aromatic substituents derivatives (**6, 7**, 14, and **15**) displayed peaks for C = O and –NH stretching in the experimental IR range.

The experimental IR spectra of the cytidine derivatives (Fig. 5) displayed peaks at almost the same frequency as the computed frequency for all the functional groups. The IR spectra of derivatives (**2** and **8**) show the following absorption bands: 1731 and 1714 cm^{-1} (due to –CO stretching), 3420 cm^{-1} and 3416 cm^{-1} (due to –OH stretching), and 3550 cm^{-1} (due to –NH stretching). Furthermore, for derivatives (**3–5**) and (**9–13**) modified with different aliphatic chains (C5–C18), the IR spectra displayed absorption bands at 1729 and 1716 cm^{-1} for C = O starching and 3470 cm^{-1} for –NH stretching. Because no –OH group was present in these derivatives, the peak for OH was absent in their spectra. Moreover, derivatives (**6**, **7**, **14**, and **15**), which comprised aromatic substituents, displayed absorption bands at 1726 and 3470 cm^{-1} corresponding to C = O and –NH stretching vibrations. Both the experimental and predicted IR analyses confirmed the insertion of different aliphatic and aromatic substituents in the cytidine structure.

MEP

In the computer-aided drug design, atomic charges are employed to investigate the connectivity between the structure and biological activity of drugs. MEP is globally used as a reactivity map displaying the most suitable regions for the electrophilic and nucleophilic attacks of charged-point-like reagents on organic molecules [46].

MEP helps interpret the biological recognition process and hydrogen bonding interactions [47]. The counter map of MEP provides a simple approach to predict how different geometries can interact. The MEP of the title compound was obtained based on B3LYP with the basis set 3-21G-optimized results (Fig. 6). MEP is important because it simultaneously displays the molecular size and shape and positive, negative, and neutral electrostatic potential regions for color grading and is useful for studying molecular structures with the physicochemical property relationship [48]. MEP was calculated to determined the reactive sites for the electrophilic and nucleophilic attacks of the optimized structure of cytidine derivatives (**7**, **8**, and **10**). The red, blue, and green colors represent the maximum negative area favorable for electrophilic attacks, maximum positive area favorable for nucleophilic attacks, and zero potential areas, respectively.

Molecular Docking Simulation

In structural biology and the computer aided drug design, molecular docking is an important computational technique. The key aim of molecular docking is to determine the potential binding geometries of a putative ligand of a known 3D structure with a target protein. In this study, several cytidine derivatives were studied *in silico* to determine their possible binding energies and interaction modes with the active sites of SARS-CoV-2 M^{pro} (Table 4) by using AutoDock Vina software. Table 3 presents the estimated binding energies of the binding site of the 6LU7 enzyme (Fig. 7) structure for all the studied compounds. According to the docking screening results, eight derivatives (**6**–**10** and **13–15**) with the strongest binding energies were selected to describe the binding mode of cytidine inhibitors. Comparatively, the aromatic derivatives exhibited better binding scores than the aliphatic derivatives. Figure 8 illustrates the interactions between the inhibitor and bordering residues of SARS-CoV-2 M^{pro} in 2D schematics acquired by importing docking results into the Discovery Studio Visualizer. These interactions showed that the amino acids participated in interactions between the ligand and enzyme with an important contribution to the total interaction energy. Most interactions included hydrophobic contacts, Van der Waals interactions, hydrogen bonding, electrostatic interactions, carbonyl interactions, and a specific atom-aromatic ring and provided insights to understand molecular recognition. Figure 9 presents the docked conformation of the most active molecules (**8** and **14**) based on the docking studies. The results showed derivative (**14**) as the most promising ligand (− 9.2 kcal/mol) that bound with SARSCoV-2 M^{pro} through hydrophobic bonding and many hydrogen interactions. The binding site is located in the hydrophobic cleft bordered with amino acid residues HIS41, ILE249, PHE294, VA104, CYS145, HIS246, and VAL297. Four hydrogen bond contacts occur with four different amino acids, ASN151, ILE152, and GLN110 at distances of 2.526, 2.814, 2.417, and 2.282 Å, respectively. Compound (**14**) exhibited an additional benzene ring in cytidine, providing a high density of electrons in the molecule and the highest binding score. These results indicated that modification of the –OH group along with long carbon chains/aromatic ring

molecules led to an increase in the binding affinity, and the addition of hetero groups such as Br caused some fluctuations in binding affinities; however, modification with halogenated aromatic rings led to an increase in the binding affinity. The docked pose showed that the drug molecules bind within the active site of the SARS-CoV-2 M^{pro} macromolecular structure.

Table 3

Binding energy of the cytidine derivatives against M^{pro}

Main protease 6LU7					**Main protease 6LU7**				
Compounds	Binding affinity	No. of hydrogen bond	No. of hydrophobic bond	NBI	Compounds	Binding affinity	No. of hydrogen bond	No. of hydrophobic bond	NBI
1	-5.9	7	1	H, A	**2**	-5.7	6	1	H, PDH, PA
3	-5.1	3	4	H, PAn, A, PA	**4**	-4.6	5	2	H, A
5	-5.5	1	3	C, A, PA	**6**	-6.1	Absent	2	PPT, PA
7	-7.4	3	3	H, PS, A	**8**	-7.4	3	3	H, PAn, PA
9	-7.4	4	9	H, PS, APS, A, PA	**10**	-7.0	5	8	H, PS, APS, A, PA
11	-5.8	3	7	H, PS, PPS, PPT, PA	**12**	-5.2	1	6	H, PS, APS, A, PA
13	-8.0	4	6	H, PS, APS, PA	**14**	-9.2	4	9	H, PS, APS, A, PA
15	-6.8	1	3	H, PS, PA					

NBI: Nonbonding interaction; H = Conventional hydrogen bond; C = Carbon–hydrogen bond; A = Alkyl; PA = Pi-alkyl; PAn = Pi-anion; APS = Amide pi-stacked; PDH = Pi-donor hydrogen bond; PPS = Pi–pi stacked; and PPT = Pi–pi T-shaped.

Parent molecule cytidine (**1**) interacted with the key residues of main protease CYS145 and HIS163 through hydrogen bonding within a close bond distance (2.173Å). Additionally, GLY143, SER144, and LEU141 interactions were observed, and interaction with SER144 showed a shorter bond distance (2.277Å) due to the unique interaction of the branched alkyl chain with the cytosine base. Acyl-chain-substituted derivatives (**3–5**) and (**11** and **12**) revealed low binding scores with the main protease, indicating the burying of the ligand in the receptor cavity. Although these derivatives exhibited low binding affinity, they interacted with the catalytic binding of the main protease, such as TYR154, HIS41, HIS163, HIS164, PHE294, GLN110, ASN238, GLU166, SER158, ILE152, THR199, and GLY143.

Table 4

Nonbonding interaction data of the cytidine derivatives against M^{pro}

Main protease 6LU7					Main protease 6LU7				
Hydrogen bond			Hydrophobic bond		Hydrogen bond			Hydrophobic bond	
Compounds	Residues	Distance (Å)	Residues	Distance (Å)	Comp.	Residues	Distance (Å)	Residues	Distance (Å)
1	LEU141	2.838	CYS145	5.085	**2**	GLY143	1.883	CYS145	5.343
	HIS163	2.663				GLU166	2.108		
	GLY143	2.483				HIS164	2.251		
	SER144	2.277				HIS163	2.398		
	SER144	2.659				LEU141	2.015		
	CYS145	2.173				HIS41	3.097		
	CYS145	2.613							
3	LYS102	2.433	ASP153	4.637	**4**	LYS137	2.737	MET276	3.937
	SER158	2.628	PRO293	4.126		LYS137	2.844	LEU287	4.611
	SER158	1.839	VAL104	5.318		LYS137	2.220		
			TYR154	5.306		THR199	2.518		
						ASN238	2.851		
5	GLN110	3.056	ILE249	5.095	**6**			TYR237	5.126
			PHE8	5.046				LEU286	5.057
			PHE294	4.595					
7	ASP289	2.119	LEU287	3.835	**8**	THR198	2.718	ASP289	3.421
	ARG131	2.329	LEU287	4.926		THR199	2.991	LEU286	4.921
	THR199	2.327	LEU286	5.198		ASN238	2.261	LEU286	4.811
9	ASN151	2.329	ILE249	3.877	**10**	ASN151	2.375	ILE249	3.984
	THR111	2.669	PHE294	4.144		ASN151	2.328	PHE294	4.225
	THR111	2.037	VAL104	3.736		THR111	2.388	ILE249	5.107
	THR111	2.611	ILE106	4.574		THR111	2.140	PRO293	4.490
			ILE249	5.080		GLN110	2.267	ILE249	4.733
			PRO293	4.611				VAL297	5.109
			VAL297	4.982				PHE294	5.480
			PHE294	5.333				PHE294	4.311
			PHE294	4.231					
11	THR111	2.680	ILE249	3.854	**12**	ILE152	2.956	ILE249	3.851
	THR111	3.081	PHE294	3.929				PHE294	4.079
	THR111	2.749	PHE294	5.516				ILE249	4.633

Main protease 6LU7					Main protease 6LU7				
			PRO293	4.744				ILE249	5.111
			VAL297	5.048				PRO293	4.326
			ILE249	4.746				VAL297	5.070
			PHE294	5.052				PHE294	3.772
13	ASN151	2.340	ILE249	3.691	**14**	ASN151	2.526	HIS41	3.834
	ASP295	2.080	PHE294	4.118		ILE152	2.417	ILE249	3.884
	ASN151	2.445	VAL297	4.998		GLN110	2.282	PHE294	4.463
	GLN110	2.116	PRO293	4.566		ASN151	2.814	ILE249	5.220
			ILE249	5.007				VAL104	3.958
			PHE294	4.415				VAL297	5.405
15	GLN110	2.068	PHE294	3.964				CYS145	4.280
			VAL104	4.881				VAL104	4.203
			ILE249	4.897				HIS246	5.103

These derivatives exhibited diverse nonbonding interactions, such as pi–anion, pi–donor hydrogen bond, amide pi-stacked, pi–pi stacked, and pi–pi T-shaped interactions, with the active sites of the main protease.

The aromatic substituents led to an increase in the binding energies in derivatives; **7–10** = − 7.4, − 7.4, − 7.4, and − 7.0 kcal/mol, respectively, and **13–15 = −** 8, − 6.2, and − 9.2 kcal/mol, respectively. These derivatives interacted with the similar binding sites of the main protease, and PHE294, THR111, GLN110, ILE249, LEU287, and ASN151 were the most common residues for them. Amongst all the proteases, GLN 110 exhibited the minimum bond distance of 2.116 and 2.068 Å. These results revealed that due to the high electron density, aromatic substituents can easily lead to an increase in the binding and antiviral abilities of the cytidine derivatives. Along with PHE294, all the derivatives showed the maximum π–π interactions with ILE249, indicating strong binding with the active site. PHE294 is considered the principal component of PPS, APS, and PPT, which is responsible for the accessibility of small molecules to the active site. Binding energies and binding modes were improved for derivatives (**7–10** and **13–15**) due to significant hydrogen bonding. The alterations of the –OH group in thymidine exalted the π–π interactions with the amino acid chain at the binding site, and their polarity improvement resulted in hydrogen bond formation. The maximum numbers of H-bonds were observed in derivative (**10**), with ASN151, THR111, and GLN110 residues.

Ten commercial medicines possibly form H-bonds with the key residues of the 2019-nCoV main protease [49]. H bonds executed a vital role in shaping the specificity of ligand binding with receptors, drug design in chemical and biological processes, molecular recognition, and biological activity. Figure 10 presents the H-bond surface and hydrophobic surface of derivative (**10**) with both the proteins. The blind docking study of all the cytidine derivatives with the SARS-CoV-2 protease revealed that the molecules were generally surrounded by the aforementioned residues, which is similar to the arrangement in standard drugs. This finding suggested that this molecule may prevent the viral replication of SARS-CoV-2.

Table 4 presents the bond distance for the ligands and the changes in the accessible area of the two important catalytic residues (Cys145 and His41) within the active site of the protease. The blind docking results revealed that all the molecules can act as potential agents for COVID treatment; however, the estimated free energies of binding values indicated derivative (**14**), with the highest negative minimum binding energy value of − 9.2 kcal/mol, as the optimum possible SARS-CoV-2 inhibitor among all the studied derivatives. Most selected cytidine derivatives exhibited promising activities and may use to develop effective antiviral drugs against SARS-CoV-2.

Biological explication

The inhibition capacity of cytidine-like nucleosides against SARS-CoV-2 M^{pro} has been investigated in vitro [33–34]. Because SARS-CoV and SARS-CoV-2 viruses are highly similar, we investigated the in silico behavior of the cytidine derivatives toward SARS-CoV-2 M^{pro}. Selecting this protein as the target led to considerable advances in antiviral treatment because it participates in the proteolytic processing of polyproteins replication. Consequently, it plays a key role in the expression and replication of viral genes. Therefore, the inhibition of this enzyme hampered the replication of the viral genome and multiplication of SARS-CoV-2. Nucleoside derivatives that can inhibit SARS-CoV $3CL^{pro}$ may inhibit SARS-CoV-2 M^{pro} in the same manner due to their high-sequence identity.

Pharmacokinetic profile and molecular radar

To predict the pharmacokinetic properties, such as solubility, lipophlicity, and toxicity of the compounds, we used the pkCSM ADMET descriptor algorithm protocol. Drug absorption depends on various factors, including membrane permeability [indicated by the cell line of colon cancer (Caco-2), intestinal absorption, skin permeability thresholds, substrate, and P-glycoprotein inhibitors.

Table 5
Prediction in silico of absorption of cytidine derivatives

Compounds	Water solubility (log mol/L)	Lipophlicity (Consensus Log $P_{o/w}$)	Caco2 permeability	Skin permeability
1	-1.689	-1.77	0.025	-2.745
2	-3.166	1.35	0.233	-2.749
3	-4.042	6.47	0.263	-2.735
4	-2.977	12.28	-0.807	-2.735
5	-2.920	13.47	-0.917	-2.735
6	-2.892	9.15	-1.732	-2.735
7	-3.616	6.95	-0.355	-2.735
8	-3.728	2.44	0.559	-2.735
9	-4.363	5.83	-0.590	-2.735
10	-4.077	6.65	-0.598	-2.735
11	-3.075	9.86	-0.625	-2.735
12	-2.951	11.23	-0.627	-2.735
13	-4.458	5.05	-0.118	-2.735
14	-2.931	6.44	0.769	-2.735
15	-2.950	5.94	0.870	-2.735

All the derivatives showed excellent lipophlicity with the values of − 1.35 to 13.47 (Table 5). Skin permeability is an important factor for drug efficacy improvement, especially in the development of transdermal drug delivery. A molecule barely penetrates the skin if log Kp is more than − 2.5 cm/h [50]. The skin permeability Kp of the cytidine derivatives is − 2.731 cm/h (< − 2.5) (Table 5). Therefore, all the presented derivatives exhibit high skin penetrability.

In the pkCSM predictive model, high Caco-2 permeability is translated into the predicted log Papp values > 0.90 cm/s.[7] The value of Caco-2 permeability (log Papp) of the cytidine derivatives ranges from − 4.3 to − 2.4 cm/s, log Papp < 0.9 cm/s (Table 6); thus, these derivatives exhibit a low Caco-2 permeability. Molecular radar is a crucial QSAR factor exhibiting the

molecular volume of compounds. Figure 11 illustrates the physicochemical radar of all the cytidine derivatives and reveals the promising QSAR features of the designed compounds. To discover oral administrative drugs, solubility is a major descriptor. High water solubility is useful to deliver active ingredients in a sufficient quantity with small volumes of pharmaceutical dosage. These water solubility values are presented as log (mol/l) (insoluble ≤ − 10 < poorly soluble < − 6 < moderately soluble < − 4 < soluble < − 2 < very soluble < 0 ≤ highly soluble). The tested compounds are soluble (Table 6).

4 Conclusions

We conducted a computational study to identify the new inhibitors of anti-SARS-CoV-2; molecular docking was studied for a series of nucleoside (cytidine) derivatives, known as anti-SARS-CoV-2 agents. All the cytidine derivatives were successfully analyzed *in silico* for their antiviral activity prediction, IR characterization, MEP calculation, molecular docking, and pharmacokinetics properties. The insertion of various aliphatic and aromatic groups in the cytidine structure can considerably improve their biological and antiviral activity modes. The experimental and computed IR peaks confirmed the presence of various aliphatic chains and aromatic groups in the cytidine structure. Antiviral prediction indicated that aliphatic (**2–4**) and aromatic (**8**, **11**, 14, and **15**) derivatives exhibit potential antiviral modes. These findings were rationalized through molecular docking, which revealed an excellent antiviral efficacy of the cytidine derivatives. Many derivatives showed outstanding binding energy and binding interactions with SARS-CoV-2 M^{pro}. Eight cytidine derivatives (**6**–**10** and **13–15**) exhibit in silico potent ability to inhibit SARS-CoV-2. Pharmacokinetic prediction provided the promising results for *in silico* properties, revealing that all the modified compounds exhibit an improved pharmacokinetic profile. Future in vitro and in vivo studies should determine whether these compounds can be drugs used to treat SARS-CoV-2.

Declarations

Acknowledgment

The authors are grateful to the Research and Publication Cell, University of Chittagong for providing financial support (*Ref.:* 21/gobe/pari/proka/doptor/C.U./2020 (dated: 22/03/2020) to carry out this research project. This work was also supported by JSPS KAKENHI under Grant No. JP19K06239 (Y.O from Yokohama City University, Japan.

Declaration of interest

The authors declare no conflict of interest.

References

1. Meanwell M, Silverman SM, Lehmann J. Adluri B, Wang Y, Cohen R, Campeau LC, Britton R (2020) A short de novo synthesis of nucleoside analogs. Science 369:725–730. https://10.1126/science.abb3231
2. Guinan M, Benckendorff C, Smith M, Miller GJ (2020) Recent advances in the chemical synthesis and evaluation of anticancer nucleoside analogues. Molecules 25:2050–2075. 10.3390/molecules25092050 https://
3. Jordheim LP, Durantel D, Zoulim F, Dumontet C (2013) Advances in the development of nucleoside and nucleotide analogues for cancer and viral diseases. Nat Rev Drug Discov 12:447–464. https://10.1038/nrd4010
4. Taylor R, Kotian P, Warren T, Panchal R, Bavari S, Julander J, Dobo S, Rose A, ElKattan Y, Taubenheim B, Babu Y, Sheridan WP (2016) BCX4430– a broad-spectrum antiviral adenosine nucleoside analog under development for the treatment of Ebola virus disease. J Infect Public Health 9:220–226. https://10.1016/j.jiph.2016.04.002
5. Pillai K, Pilay V, Jasamai M, Thayan R, Santhanam J, Hassan SS, Yap WB (2017) Nucleoside analogs as potential antiviral agents for dengue virus infections. Med Chem Res 26:1382–1387. https://10.1007/s00044-017-1863-4
6. Eyer L, Nencka R, Huvarová I, Palus M, Alves MJ, Gould EA, De Clercq E, Růžek D (2016) Nucleoside inhibitors of Zika virus. J Infect Dis 214:707–711. https://10.1093/infdis/jiw226

7. Hamuy R, Berman B (1998) Topical antiviral agents for herpes simplex virus infections. Drug Today 34:1013–1025. https://10.1358/dot.1998.34.12.487486
8. Rabasseda X (2003) Brivudine: A herpes virostatic with rapid antiviral activity and once-daily dosing. Drugs Today 39:359–371. https://10.1358/dot.2003.39.5.740221
9. Yuen GJ, Weller S, Pakes GE (2008) A review of the pharmacokinetics of abacavir. Clin Pharmacokinet 47:351–371. https://10.2165/00003088-200847060-00001
10. Kawsar SMA, Islam M, Jesmin S, Manchur MA, Hasan I, Rajia S (2018) Evaluation of the antimicrobial activity and cytotoxic effect of some uridine derivatives. Int J Biosci 12:211–219. http://dx.doi.org/10.12692/ijb/12.6.211-219
11. Kawsar SMA, Hamida AA, Sheikh AU, Hossain MK, Shagir AC, Sanaullah AFM, Manchur MA, Imtiaj H, Ogawa Y, Fujii Y, Koide Y, Ozeki Y (2015) Chemically modified uridine molecules incorporating acyl residues to enhance antibacterial and cytotoxic activities. Int J Org Chem 5:232–245. https://doi.org/10.4236/ijoc.2015.54023
12. Shagir AC, Bhuiyan MMR, Ozeki Y, Kawsar SMA (2016) Simple and rapid synthesis of some nucleoside derivatives: structural and spectral characterization. Curr Chem Lett 5:83–92. https://doi.org/10.5267/j.ccl.2015.12.001
13. Maowa J, Alam A, Rana KM, Dey S, Hosen A, Fujii Y, Hasan I, Ozeki Y, Kawsar SMA (2021a) Synthesis, characterization, synergistic antimicrobial properties and molecular docking of sugar modified uridine derivatives. Ovidius Univ Annal Chem 32:6–21. https://doi.org/10.2478/auoc-2021-0002
14. Bulbul MZH, Chowdhury TS, Misbah MMH, Ferdous J, Dey S, Hasan I, Fujii Y, Ozeki Y, Kawsar SMA (2021a) Synthesis of new series of pyrimidine nucleoside derivatives bearing the acyl moieties as potential antimicrobial agents. Pharmacia 68:23–34. https://doi.org/10.3897/pharmacia.68.e56543
15. Arifuzzaman M, Islam MM, Rahman MM, Mohammad AR, Kawsar SMA (2018) An efficient approach to the synthesis of thymidine derivatives containing various acyl groups: characterization and antibacterial activities. ACTA Pharm Sci 56:7–22. https://doi.org/10.23893/1307-2080.APS.05622
16. Mirajul MI, Arifuzzaman M, Monjur MR, Atiar MR, Kawsar SMA (2019) Novel methyl 4,6-*O*-benzylidene-α-D-glucopyranoside derivatives: synthesis, structural characterization and evaluation of antibacterial activities. Hacettepe J Biol Chem 47:153–164. https://doi.org/10.15671/hjbc.622038
17. Kawsar SMA, Ferdous J, Mostafa G, Manchur MA (2014a) A synthetic approach of D-glucose derivatives: spectral characterization and antimicrobial studies. Chem Chem Technol 8:19–27. https://doi.org/10.23939/chcht08.01.019
18. Misbah MMH, Ferdous J, Bulbul MZH, Chowdhury TS, Dey S, Hasan I, Kawsar SMA (2020) Evaluation of MIC, MBC, MFC and anticancer activities of acylated methyl β-D-galactopyranoside esters. Int J Biosci 16:299–309. http://dx.doi.org/10.12692/ijb/16.4.299-309
19. Alam A, Hosen MA, Islam M, Ferdous J, Fujii Y, Ozeki Y, Kawsar SMA (2021) Synthesis, Antibacterial and cytotoxicity assessment of modified uridine molecules. Curr Adv Chem Biochem 6:114–129. doi:https://10.9734/bpi/cacb/v6/8670D
20. Kawsar SMA, Kumar A (2021) Computational investigation of methyl α-D-glucopyranoside derivatives as inhibitor against bacteria, fungi and COVID-19 (SARS-2). J Chilean Chem Soc 66:5206–5214
21. Kawsar SMA, Faruk MO, Rahman MS, Fujii Y, Ozeki Y (2014b) Regioselective synthesis, characterization, and antimicrobial activities of some new monosaccharide derivatives. Sci Pharm 82:1–20. https://doi.org/10.3797/scipharm.1308-03
22. Yasmin F, Amin MR, Hosen MA, Bulbul MZH, Dey S, Kawsar SMA (2021) Bromobenzoylation of methyl α-D-mannopyranoside: synthesis and spectral characterization. J Sib Fed Univ Chem 14:171–1838. https://10.17516/1998-2836-0226
23. Ching-Lung L, Edward G, Yun-Fan L, Chao-Wei H, Satawat T, Yuming W, Yagang C, Heathcote EJ, Rasenack J, Natalie B, Nikolai VN, Adrian MDB, Stefan Z, Young MM, Zachary G, George C, Barbara FC, Nathaniel AB (2007) Telbivudine Versus Lamivudine in Patients With Chronic Hepatitis B. N Engl J Med 357:2576–2588. https://10.1056/NEJMoa066422
24. Teather LA, Wurtman RJ (2003) Dietary cytidine (5′)-diphosphocholine supplementation protects against development of memory deficits in aging rats. Prog Neuro-psychopharmacol Biol *Psych* 27:711–717 https:// 10.1016/S0278-5846(03)00086-1

25. Rana KM, Ferdous J, Hosen A, Kawsar SMA (2020) Ribose moieties acylation and characterization of some cytidine analogs. J Sib Fed Univ Chem 13:465–478. https://doi.org/10.17516/1998-2836-0199
26. Alam A, Hosen MA, Hosen A, Fujii Y, Ozeki Y, Kawsar SMA (2021) Synthesis, characterization, and molecular docking against a receptor protein FimH of *Escherichia coli* (4XO8) of thymidine derivatives. J Mexican Chem Soc 65:256–276. https://doi.org/10.29356/jmcs.v65i2.1464
27. Devi SR, Jesmin S, Rahman M, Manchur MA, Fujii Y, Kanaly RA, Ozeki Y, Kawsar SMA (2019) Microbial efficacy and two step synthesis of uridine derivatives with spectral characterization. ACTA Pharm Sci 57:47–68. https://doi.org/10.23893/1307-2080.APS.05704
28. Kawsar SMA, Hosen MA, Fujii Y, Ozeki Y (2020a) Thermochemical, DFT, molecular docking and pharmacokinetic studies of methyl β-D-galactopyranoside esters. J Comput Chem Mol Model 4:452–462. https://dx.doi.org/10.25177/JCCMM.4.4.RA.10663
29. Kawsar SMA, Hosen MA (2020b) An optimization and pharmacokinetic studies of some thymidine derivatives. Turkish Comput Theor Chem 4:59–66. https://doi.org/10.33435/tcandtc.718807
30. Bartolucci S, Estenoz M, Franciscis VD, Carpinelli P, Colucci GL, Tocco GA, Rossi M (1989) Effect of cytidine analogs on cell growth and differentiation on a human neuroblastoma line. Cell Biophys 15:67–77. https://10.1007/BF02991580
31. Harris KS, Brabant W, Styrchak S, Gall A. Daifuku R (2005) KP-1212/1461, a nucleoside designed for the treatment of HIV by viral mutagenesis. *Antiviral* Res 67:1–9. https://10.1016/j.antiviral.2005.03.004
32. Lu H (2020) Drug treatment options for the 2019-new coronavirus (2019-nCoV). Biosci Trends 14:69–71. https://10.5582/bst.2020.01020
33. Maowa J, Hosen MA, Alam A, Rana KM, Fujii Y, Ozeki Y, Kawsar SMA (2021b) Pharmacokinetics and molecular docking studies of uridine derivatives as SARS- COV-2 M^{pro} inhibitors. Phys Chem Res 9:385–412. https://doi.org/10.22036/pcr.2021.264541.1869
34. Bulbul MZH, Hosen MA, Ferdous J, Chowdhury TS, Misbah MMH, Kawsar SMA (2021b) Thermochemical, **DFT study, physicochemical, molecular docking and ADMET predictions of some modified uridine derivatives.**. Int J New Chem 8:88–110. https://doi.org/10.22034/ijnc.2020.131337.1124
35. Seeberger PH, Werz DB (2007) Synthesis and medical applications of oligosaccharides. Nature 446:1046–1051. https://doi.org/10.1038/nature05819
36. Frisch MJ, Trucks GW, Schlegel HB, Scuseria GE, Robb A, Cheeseman JR, Scalmani G, Barone V, Mennucci M, Petersson GA et al (2009) Gaussian 09. Gaussian Inc, Wallingford. https://gaussian.com/g09citation/
37. Becke AD (1988) Density-functional exchange-energy approximation with correct asymptotic behaviour. Phy Rev A 38:3098–3100. https://doi.org/10.1103/physreva.38.3098
38. Lee C, Yang W, Parr RG (1988) Development of the Colle-Salvetti correlation-energy formula into a functional of the electron density. *Phys Rev* B 37:785–789. https://doi.org/10.1103/physrevb.37.785
39. Cheng F, Li W, Zhou Y, Shen J, Wu Z, Liu G, Lee PW, Tang Y (2012) admetSAR: A comprehensive source and free tool for assessment of chemical ADMET properties. J Chem Inform Model 52:3099–3105. https://doi.org/10.1021/ci300367a
40. Berman HM, Westbrook J, Feng Z, Gilliland G, Bhat TN, Weissig H, Shindyalov IN, Bourne PE (2000) The protein data bank. Nucleic Acids Res 28:235–242. https://doi.org/10.1093/nar/28.1.235
41. Delano WI (2002) The PyMOL molecular graphics system. De-Lano Scientific, San Carlos
42. Guex N, Peitsch MC (1997) SWISS-MODEL and the Swiss-PdbViewer: an environment for comparative protein modeling. Electrophoresis 18:2714–2723. https://doi.org/10.1002/elps.1150181505
43. Williams CH, Hong CC (eds) (2015) Chemical biology: methods and protocols. Springer, New York. https://10.1007/978-1-4939-2269-7
44. Version ADS (2017) 4.0. Accelrys, San Diego
45. Yasmin F, Amin MR, Hosen MA, Bulbul MZH, Dey S, Kawsar SMA (2021) Monosaccharide derivatives: synthesis, antimicrobial, pass, antiviral, and molecular docking studies against sars-cov-2 m^{pro} inhibitors. Cellu Chem Technol

55:477–499

46. Amin ML (2013) P-glycoprotein inhibition for optimal drug delivery. Drug Target Insights 7:27–34. https://doi.org/10.4137/DTI.S12519
47. Politzer P, Murray JS (1991) Molecular electrostatic potentials and chemical reactivity. Rev Comput Chem 2:273–312. https://doi.org/10.1002/9780470125793.ch7
48. Politzer P, Truhlar DG (eds) (1981) Chemical applications of atomic and molecular electrostatic potentials. Reactivity, Structure, Scattering, and Energetics of Organic, Inorganic, and Biological Systems. Springer, USA https://www.springer.com/gp/book/9780306406577
49. Liu X, Wang XJ (2020) Potential inhibitors against 2019-nCoV coronavirus M protease from clinically approved medicines. J Genet Genom 7:119–121. https://10.1016/j.jgg.2020.02.001
50. Lipinski CA, Lombardo F, Dominy BW, Feeney PJ (2001) Experimental and computational approaches to estimate solubility and permeability in drug discovery and development. *Adv Drug Deliv* Rev 46:3–26. https://doi.org/10.1016/s0169-409x(00)00129-0

Figures

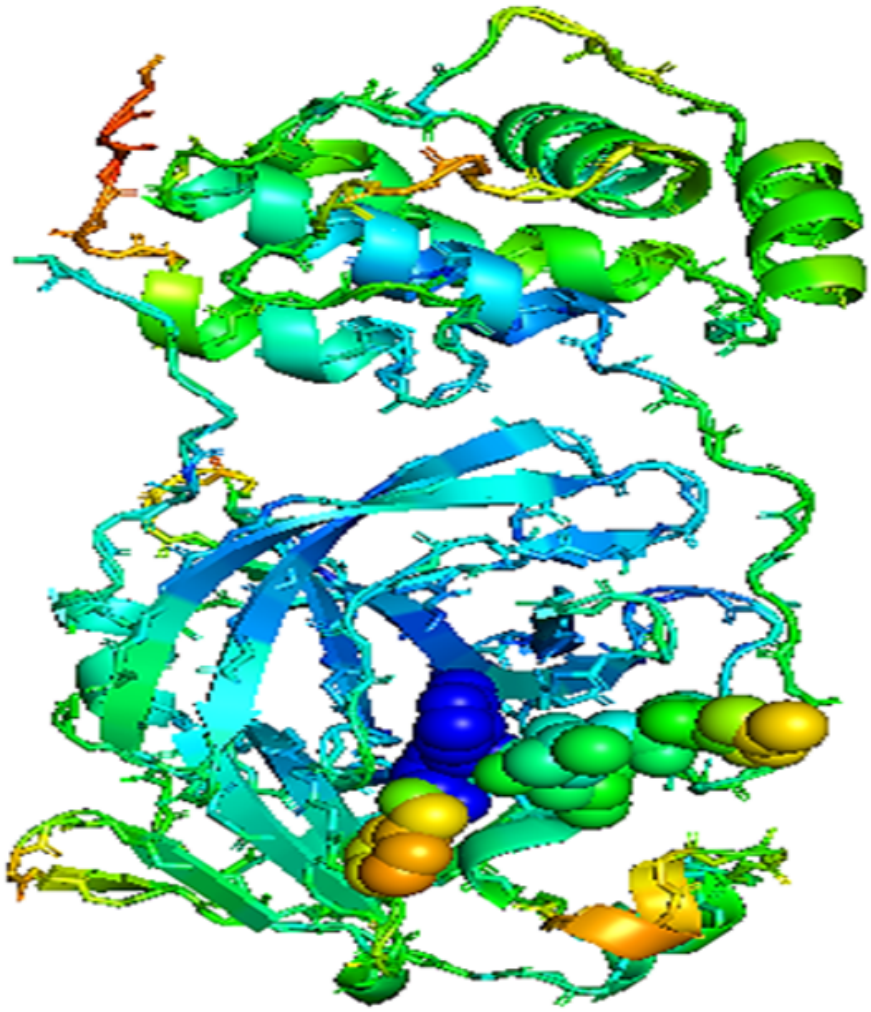

Figure 1

Crystal structure of the SARS CoV-2 main protease protein (pdb: 6LU7) with the binding pocket

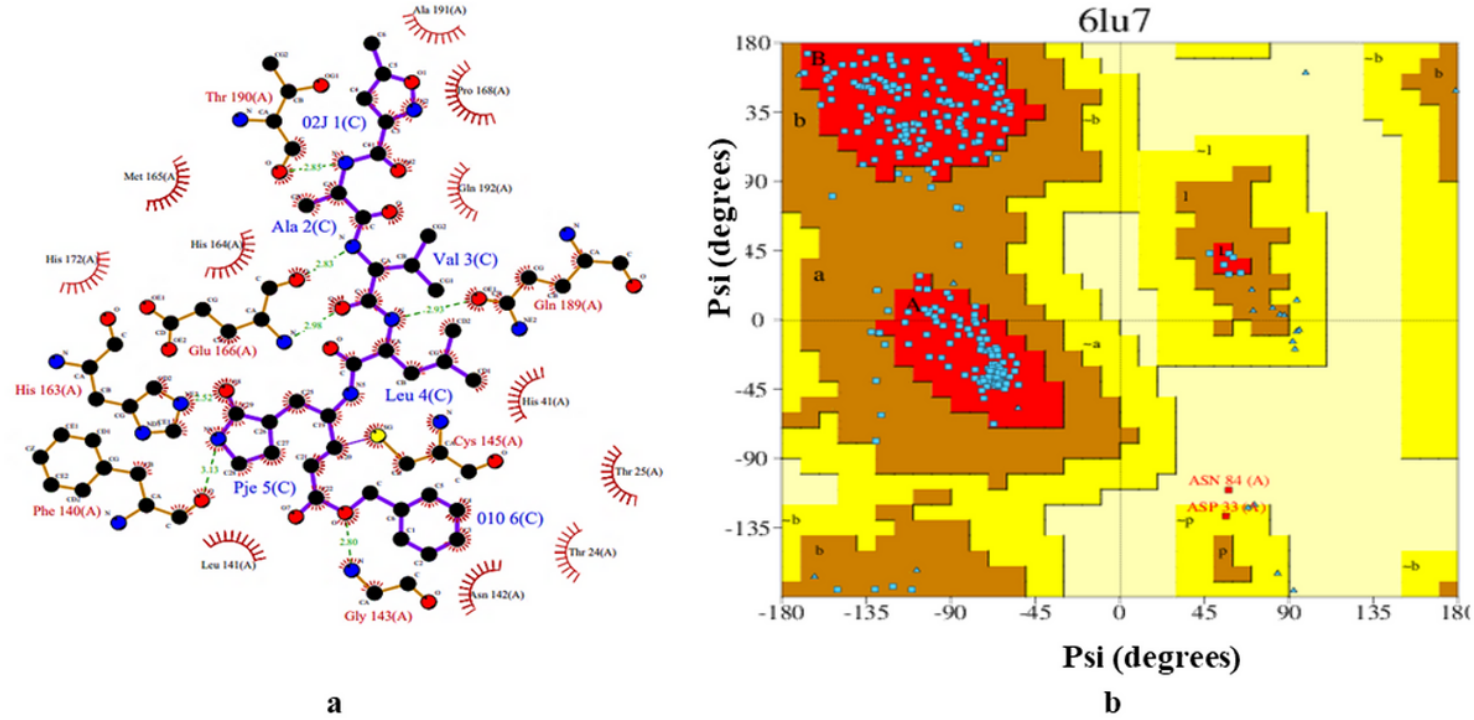

Figure 2

(a) Ligplot and (b) Ramachandran plot of the SARS CoV-2 main protease protein (pdb: 6LU7)

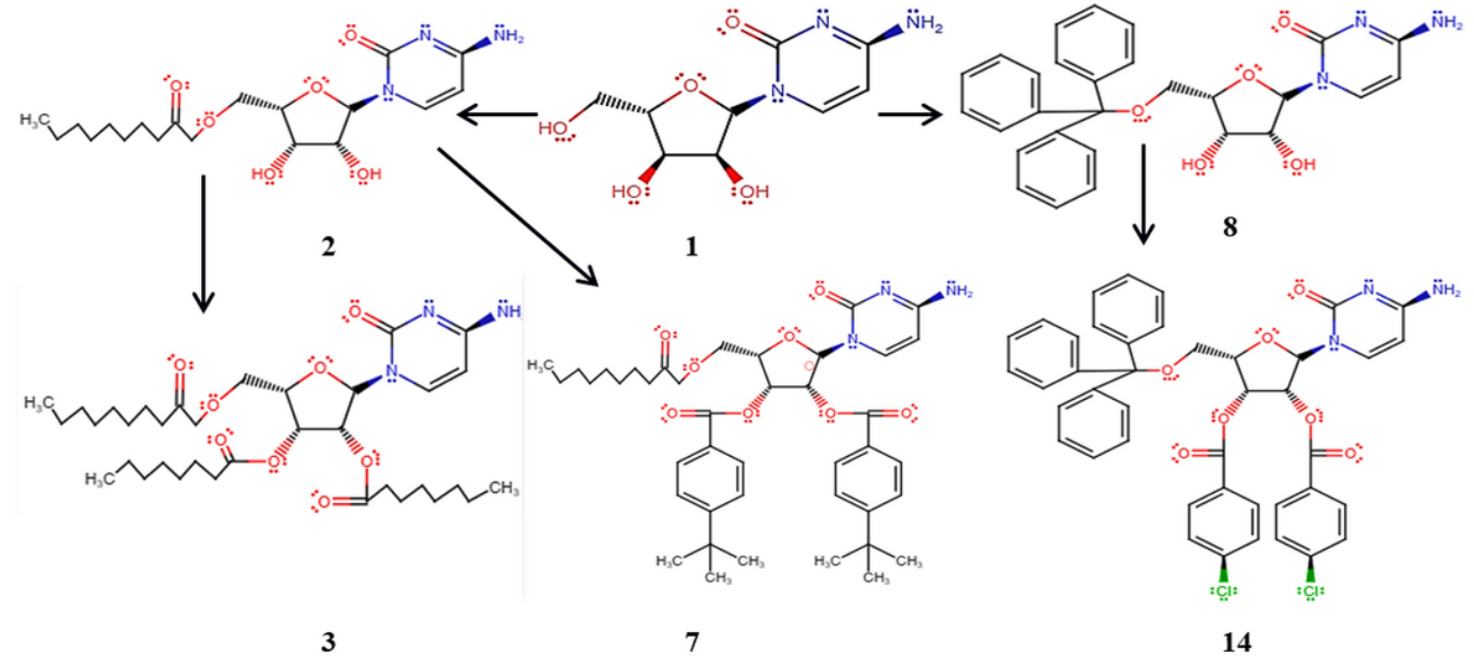

Figure 3

2D structure of designed cytidine (1) and its derivatives (2, 3, 7, 8, and 14)

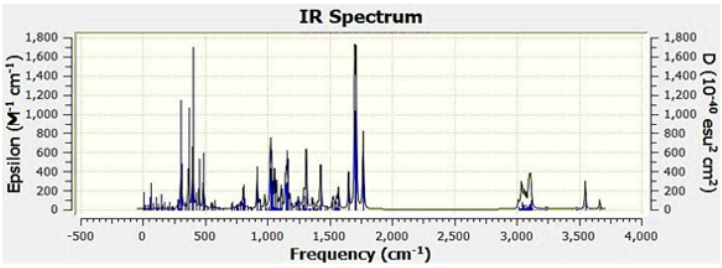

2

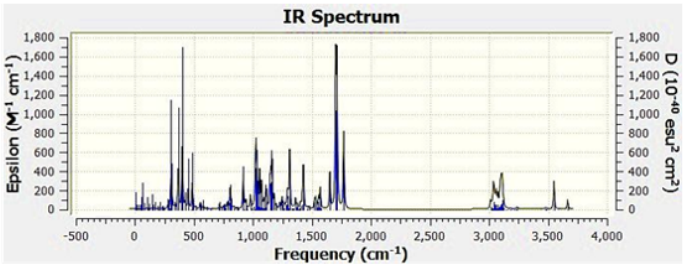

3

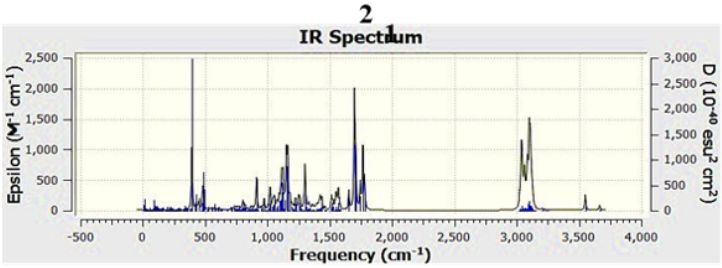

4

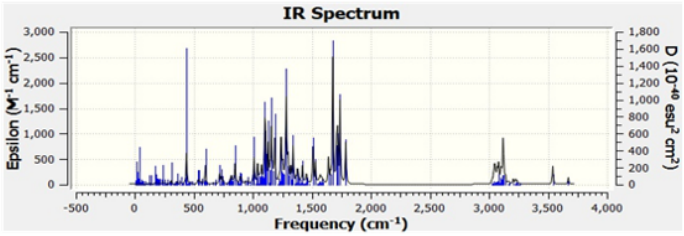

7

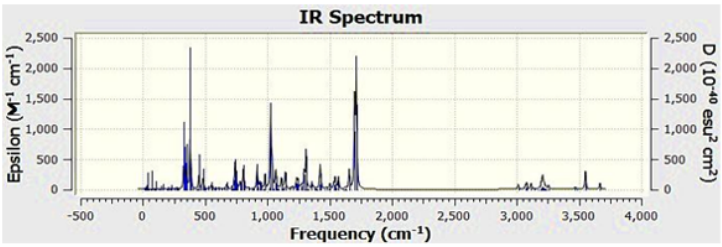

8

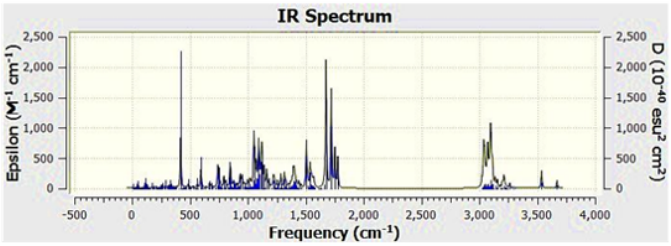

12

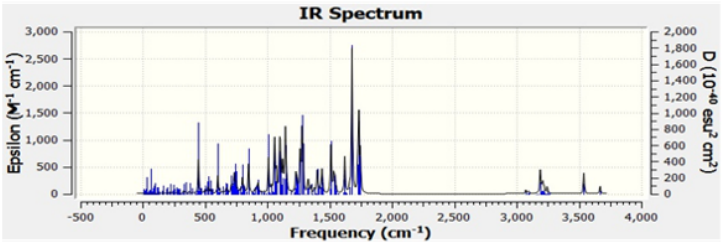

14

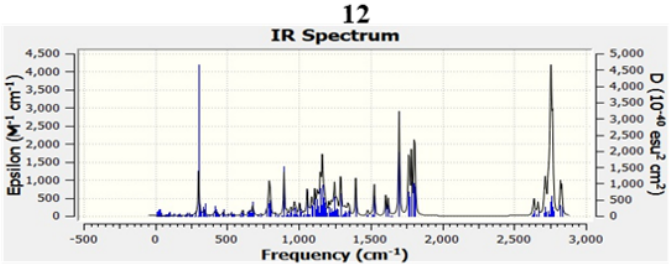

15

Figure 4

Computing IR spectrum from Gaussian base on DFT-B3LYP/3-21G

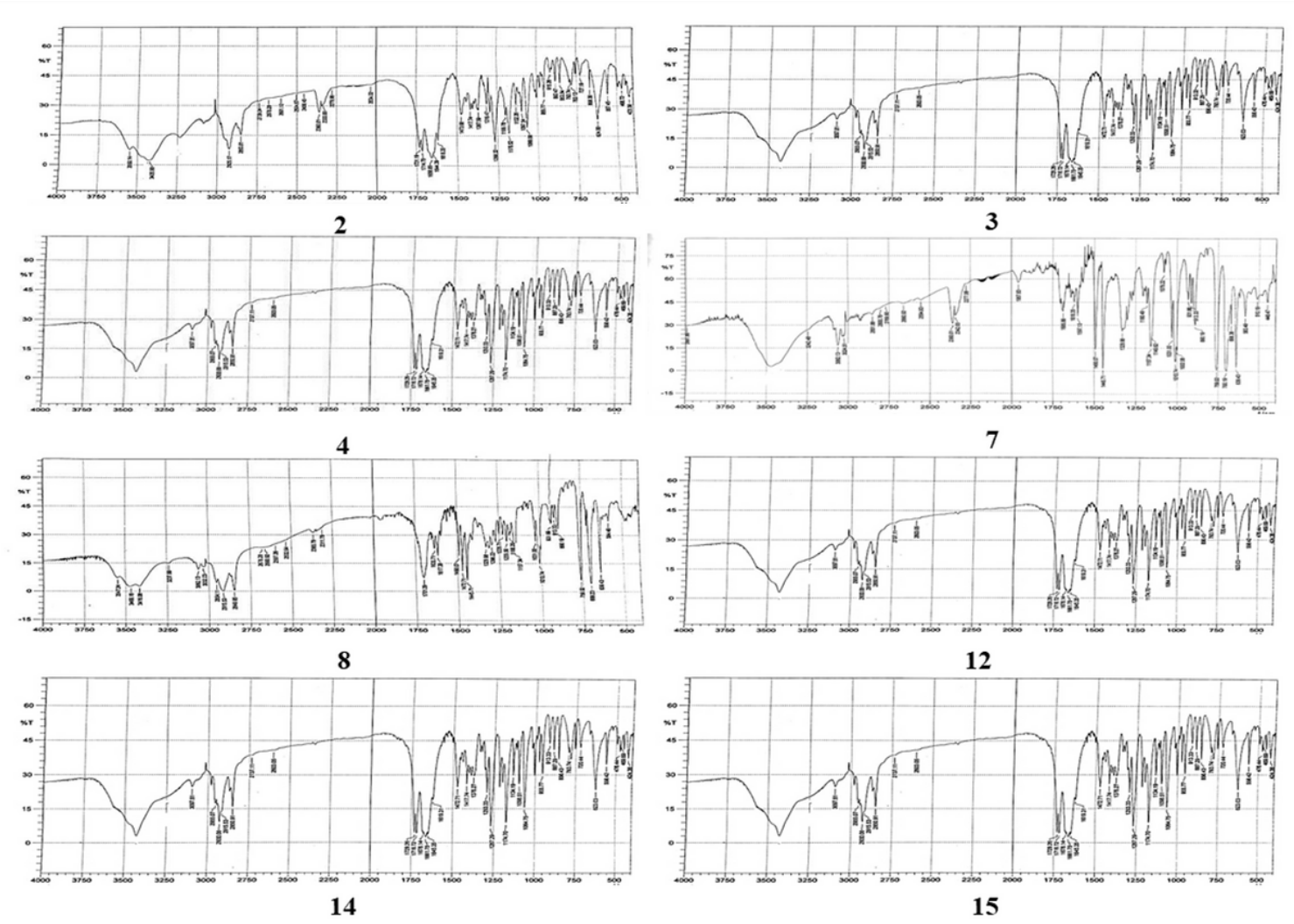

Figure 5

Experimental IR spectra of the cytidine derivatives (2–4, 7, 8, 12, 14, and 15)

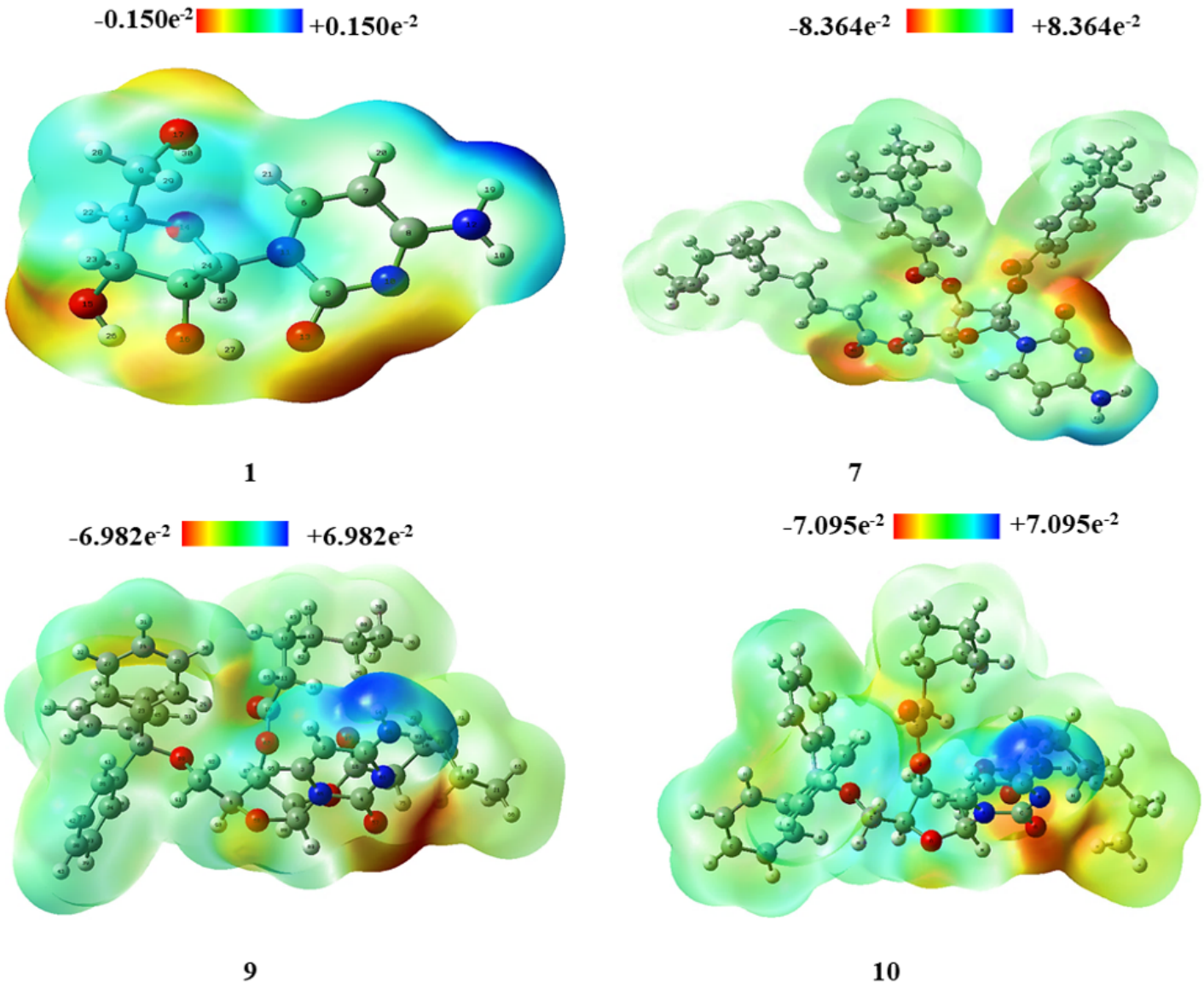

Figure 6

MEP map of cytidine (1) and its derivatives (7, 8, and 10)

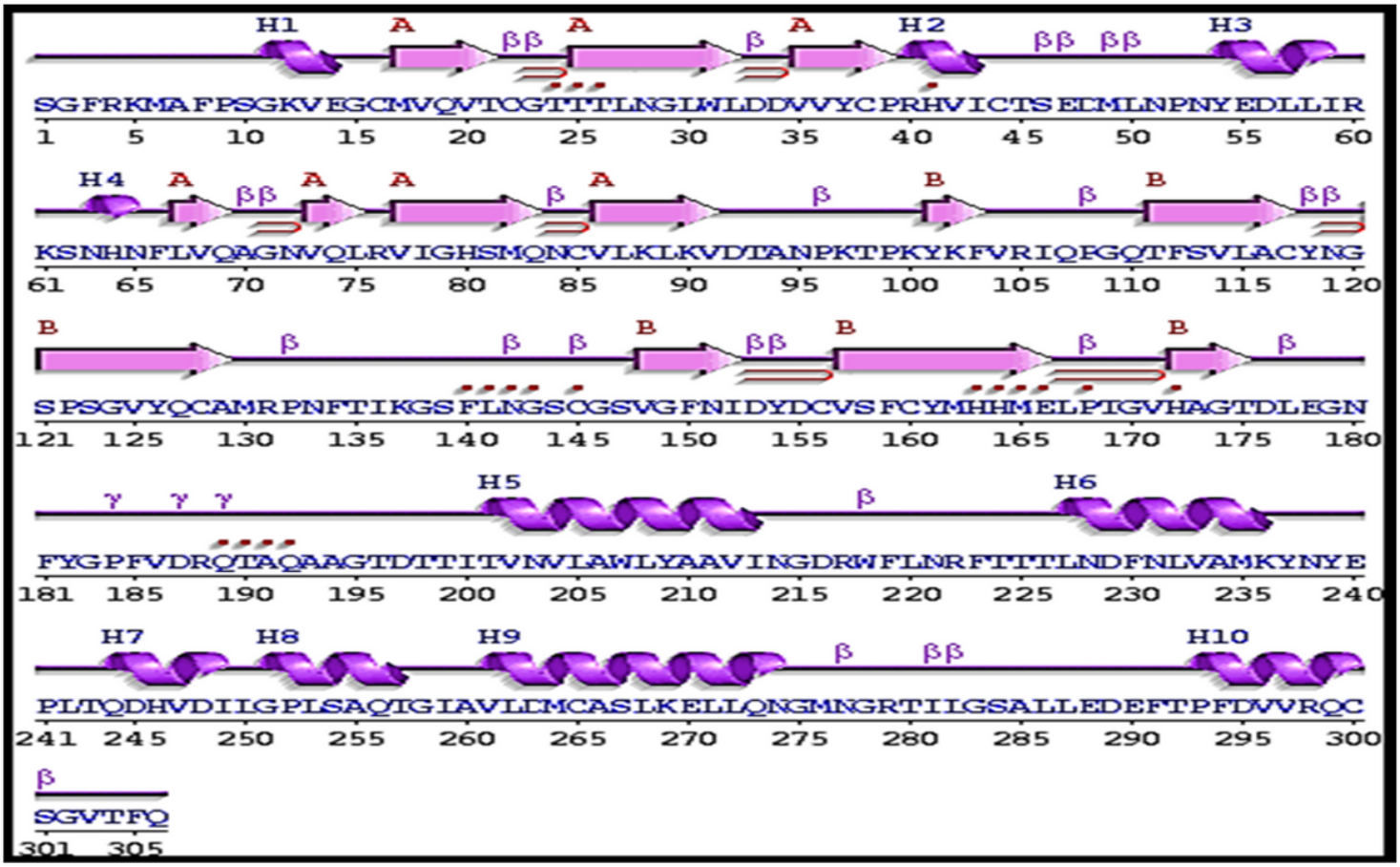

Figure 7

Multiple sequence alignment of the closest homologs of Mpro (PDB: 6LU7)

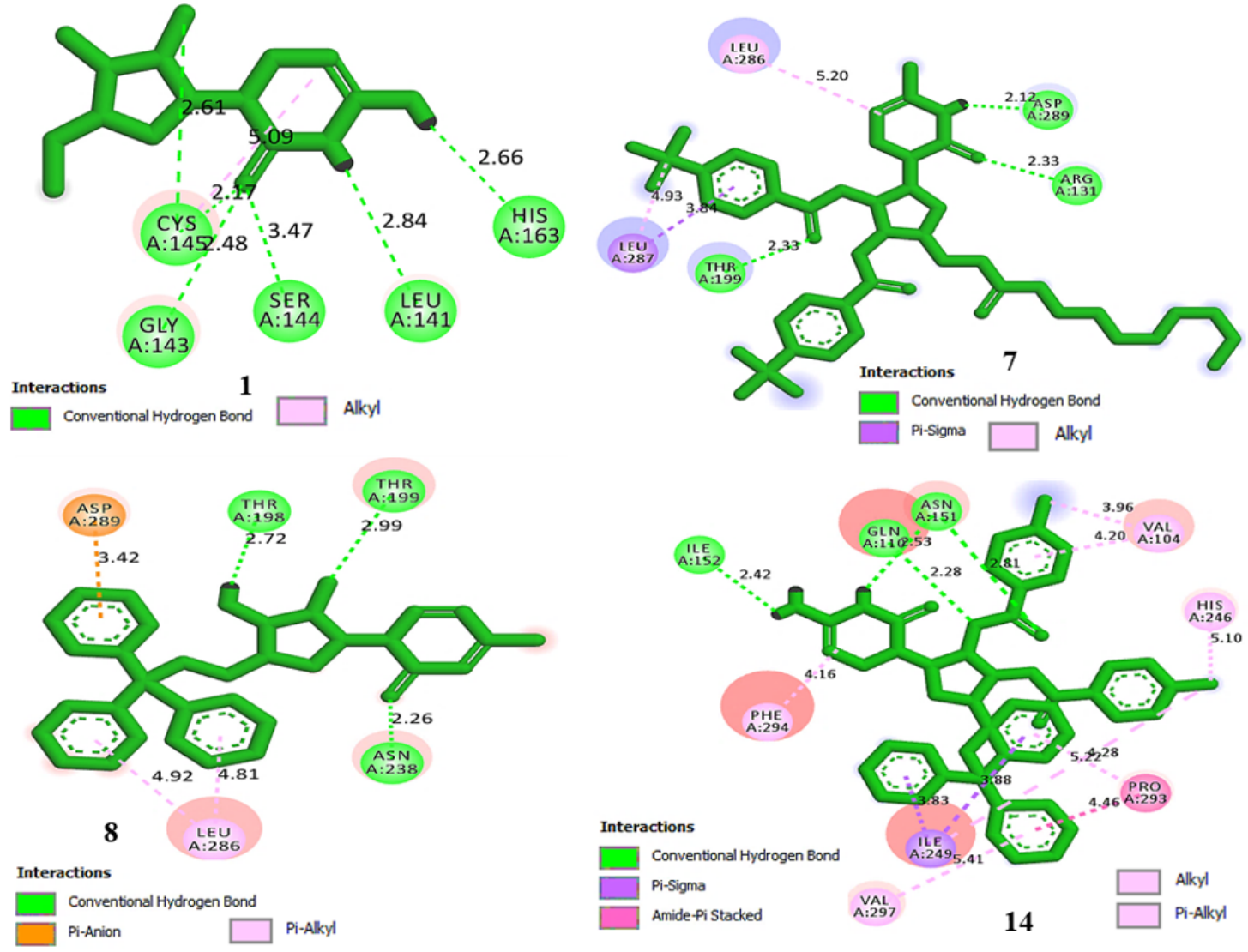

Figure 8

Nonbonding interactions of derivatives (1, 7, 8, and 14) with the active site of SARS-CoV-2 (PDB: 6LU7) performed by Discovery Studio

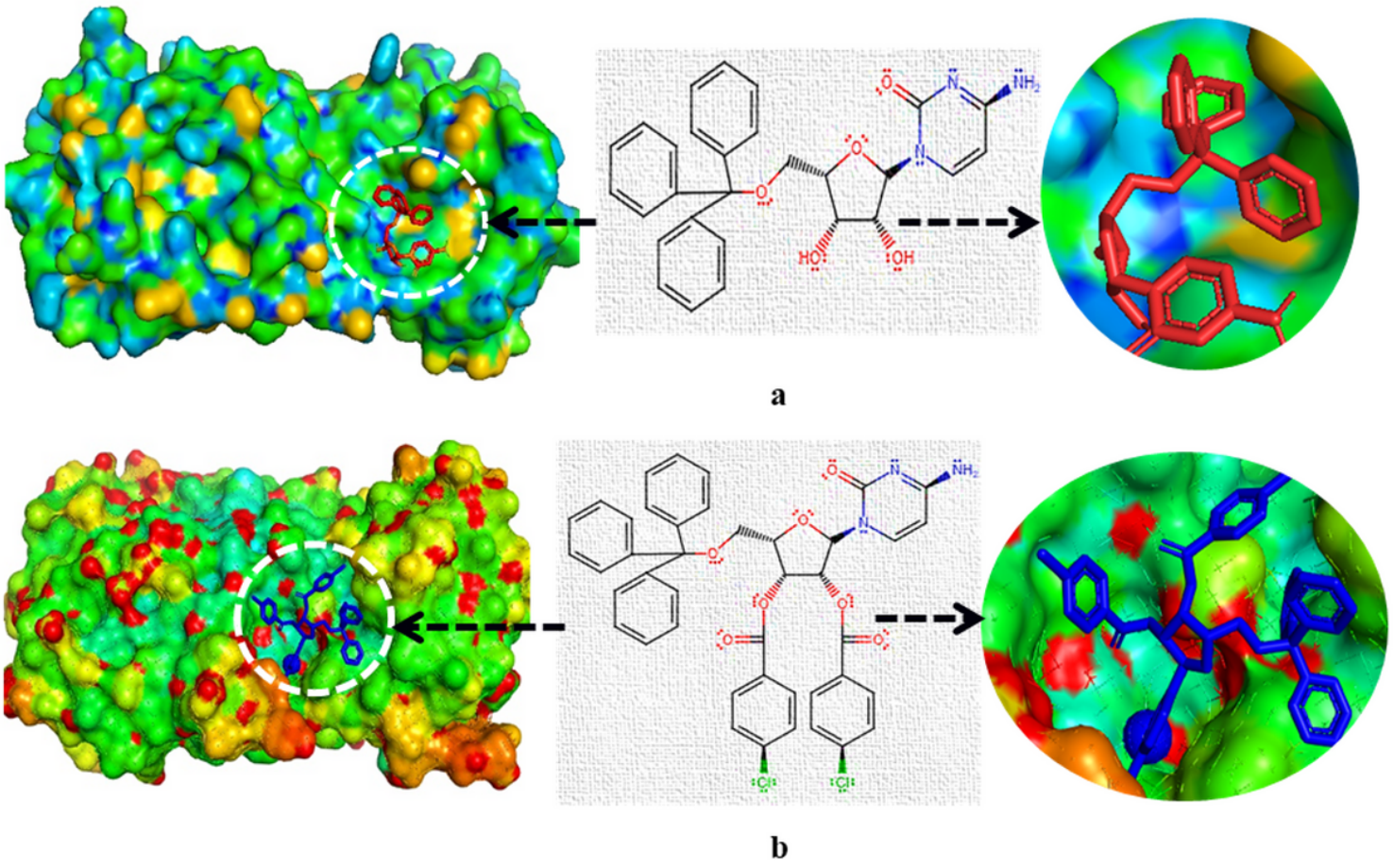

Figure 9

(a) Docked 2D pose of derivative 8 with Mpro (PDB: 6LU7) (b); Docked 2D pose of derivative 14 with Mpro (PDB: 6LU7)

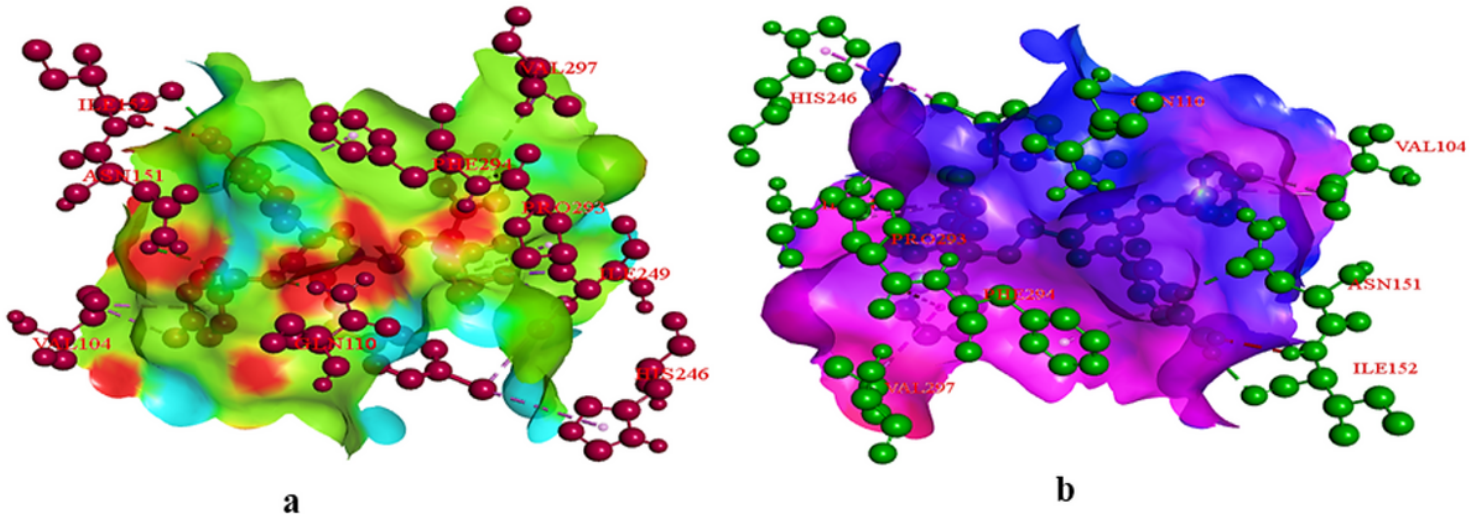

Figure 10

(a) Hydrogen bond surface of SARS-CoV-2 (PDB: 6LU7) derivative 10 (b); hydrophobic bond surface of SARS-CoV-2 (PDB: 6LU7) with derivative 10

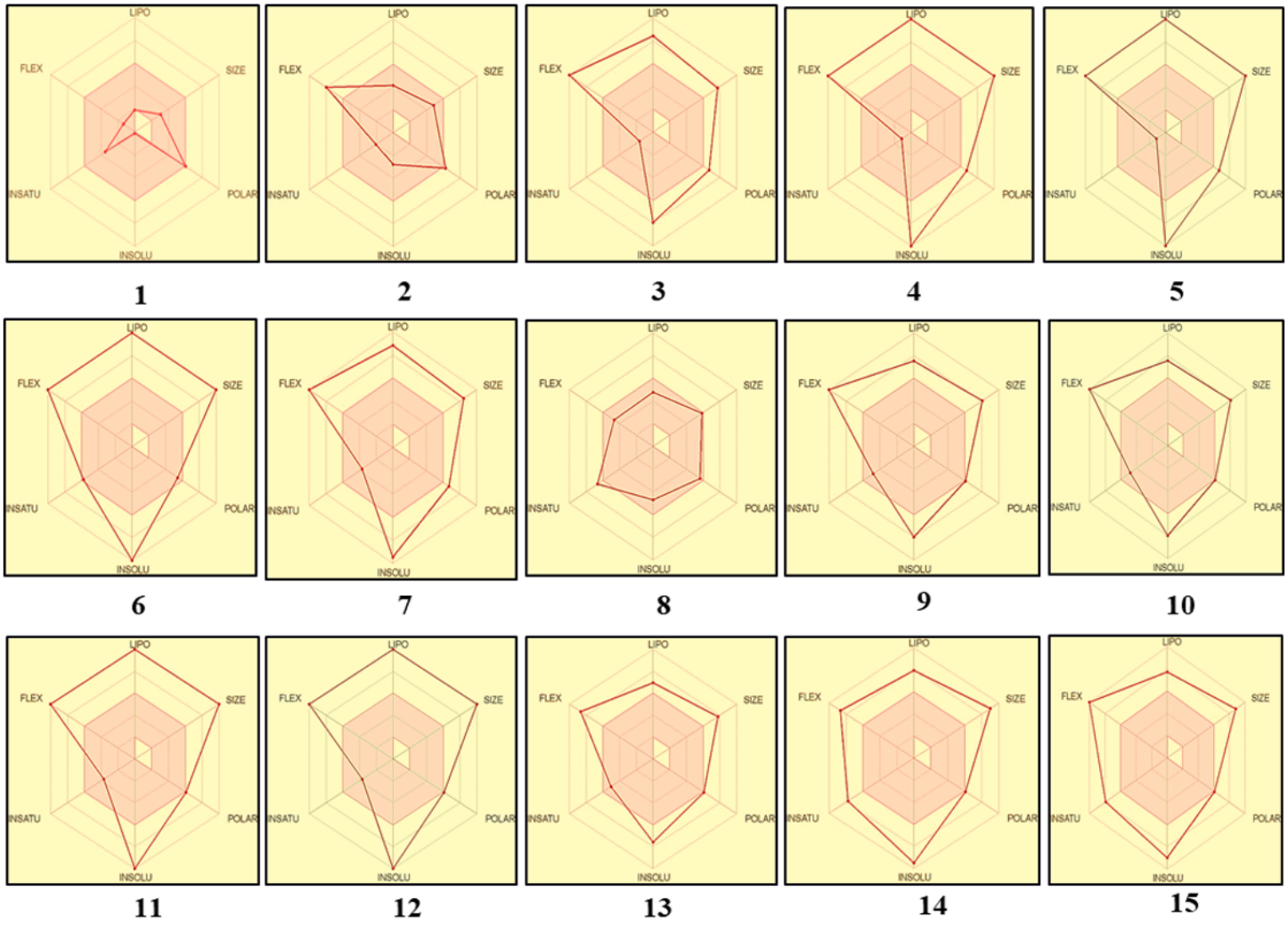

Figure 11

Bioactivity radar Charts of the thymidine derivatives where FLEX: Flexibility, LIPO: Lipophilicity, INSATU: Insaturation. and INSOLU: Insolubility

Supplementary Files

This is a list of supplementary files associated with this preprint. Click to download.

- KawsaretalSupplementarymaterial.docx